Analytical Impedance of Oxygen Transport in a PEM Fuel Cell Channel

Andrei Kulikovsky [1,2,*,z]

[1] *Forschungszentrum Jülich GmbH Institute of Energy and Climate Research, Electrochemical Process Engineering, D-52425 Jülich, Germany*
[2] *Lomonosov Moscow State University, Research Computing Center, 119991 Moscow, Russia*

We report a model for impedance Z_h of oxygen transport in a PEMFC channel. Analytical solution for Z_h is derived and a simple approximate equation for the summit frequency of Z_h arc is obtained. In the limit of zero frequency of AC signal, a rather cumbersome expression for Z_h reduces to a simple equation for the cell resistivity due to oxygen transport in the channel: $R_h = -b\left(J(\lambda-1)\ln\left(1-\frac{1}{\lambda}\right)\right)^{-1} - \frac{b}{J}$, where b is the ORR Tafel slope per exponential basis, λ is the stoichiometry of the oxygen (air) flow, and J is the mean current density in the cell.
 [DOI: 10.1149/2.0951904jes]

Manuscript submitted November 5, 2018; revised manuscript received February 13, 2019. Published March 6, 2019.

Impedance of a polymer electrolyte membrane fuel cell (PEMFC) contains invaluable information on cell transport and kinetic coefficients. Nowadays, measuring cell impedance is a routing procedure; however, analysis of impedance spectra is a non–trivial task requiring relevant physics–based models.

Impedance spectrum of a PEMFC operating at a low oxygen stoichiometry contains a large low–frequency (LF) arc exhibiting the impedance due to oxygen transport in the air channel. In local spectra, the diameter of this arc increases with the distance from inlet due to oxygen exhaustion along the channel. Schneider et al.[1,2] were the first who emphasized importance of this "forgotten player" for spectra analysis and provided detailed experimental study of local impedance in a segmented cell. Further modeling efforts[3–7] have led to development of analytical and numerical models, which included the "channel" impedance of a PEMFC. The distribution of local cell parameters along the cathode channel is of great interest for cell designers and a lot of efforts have been done to construct and employ the techniques for local impedance measurements.[8–11]

Numerical model for impedance of the transport electrode with accurate account of the axial and longitudinal reactant diffusion and of the parabolic flow velocity profile in the channel cross section has been developed by Holm et al.[12] Bao and Bessler developed a numerical model for PEMFC impedance based on their CFD transient model for cell performance which included oxygen transport in the channel.[4]

To achieve a reasonable balance between the model complexity and speed of calculations, the models[5–7] employ a simplifying assumption of plug flow conditions in the channel. Yet, however, these models include numerical boundary–value solvers and a procedure for least–squares fitting of impedance equations to experimental spectra. A simple analytical equation for estimation of the channel impedance and, in particular, of the channel resistivity would be very desirable. Chevalier et al.[13] developed a model for determination of air flow velocity in the PEMFC channel from the LF impedance arc. Recently, Chevalier et al.[14] derived an asymptotic solution for the LF arc and compared this solution to impedance measurements.

In this work, we report a model for the channel impedance in a PEM fuel cell. The model yields an analytical solution for this impedance; in the limit of zero frequency of the exciting signal a simple expression for the channel resistivity is derived.

Characteristic Frequencies of PEMFC Impedance

The assumptions behind the PEMFC impedance model below are based on the estimates of characteristic frequencies of the faradaic and transport processes in the cell. Consider a PEM fuel cell with the single straight channel running with air on the cathode side (Figure 1); let this cell be operated at a low current density J:

$$J \ll \min\left\{ j_p = \frac{\sigma_p b}{l_t},\quad j_{ox} = \frac{4FD_{ox}c_1}{l_t} \right\} \qquad [1]$$

where σ_p is the cathode catalyst layer (CCL) proton conductivity, b is the ORR tafel slope per exponential basis, l_t is the CCL thickness, D_{ox} is the effective oxygen diffusion coefficient in the CCL, and c_1 is the oxygen concentration at the CCL/GDL interface. Eq. 1 means that the cell current density must be much less than the characteristic current densities for proton j_p and oxygen j_{ox} transport in the CCL.[15] With the typical PEMFC parameters Eq. 1 limits J by 100 mA cm^{-2}.

The characteristic frequency ω_p of proton transport in the CCL can be estimated as the inverse time constant of a parallel RC–circuit with $R = R_p$ and $C = C_{dl}l_t$. Here $R_p = l_t/(3\sigma_p)$ is the proton transport resistivity,[16] and C_{dl} is the volumetric double layer capacitance. For ω_p, we, thus, have

$$\omega_p \simeq \frac{3\sigma_p}{C_{dl}l_t^2} \qquad [2]$$

The characteristic frequency ω_{ct} of the faradaic (charge–transfer) process in the CCL is given by $(R_{ct}C_{dl}l_t)^{-1}$, where $R_{ct} = b/J$ is the charge–transfer resistivity and J is the mean current density in the cell:

$$\omega_{ct} = \frac{J}{bC_{dl}l_t} \qquad [3]$$

The characteristic frequencies of oxygen transport in the CCL ω_{ox} and in the GDL ω_b can be estimated as the characteristic frequency of a

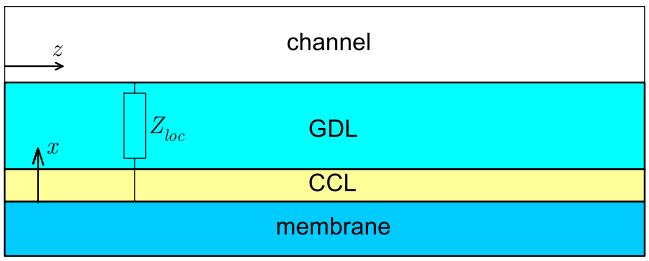

Figure 1. Schematic of the cell and the system of coordinates. CCL and GDL abbreviate the cathode catalyst layer, and the gas diffusion layer, respectively. Z_{loc}, in general, includes the CCL and GDL impedances; however, in this work the oxygen and proton transport impedances are neglected (see the text).

*Electrochemical Society Member.
[z]E-mail: A.Kulikovsky@fz-juelich.de

Table I. Cell geometrical and operating parameters used in the calculation of the characteristic frequencies shown in the lower part of the Table. The characteristic values of D_{ox}, D_b b, σ_p and C_{dl} are taken from impedance measurements;[18] the value of i_* is assumed. The Tafel slope is given per exponential basis.

Catalyst layer thickness l_t, cm	10^{-3}
Gas diffusion layer thickness l_b, cm	0.025
Oxygen diffusion coefficient in the CCL D_{ox}, cm^2 s^{-1}	10^{-4}
Oxygen diffusion coefficient in the GDL D_b, cm^2 s^{-1}	10^{-2}
Exchange current density i_*, A cm^{-3}	10^{-3}
ORR Tafel slope b, V	0.03
CCL proton conductivity σ_p, Ω^{-1} cm^{-1}	0.03
Double layer capacitance, C_{dl}, F cm^{-3}	20
Channel length L, cm	100
Channel depth h, cm	0.1
Flow velocity in the channel v, cm s^{-1}	36.2
Cell temperature T, K	273 + 80
Mean cell current density J, A cm^{-2}	0.05
Air flow stoichiometry λ	2
ω_p, s^{-1}	4500
ω_{ct}, s^{-1}	83.3
ω_{ox}, s^{-1}	254
ω_b, s^{-1}	40.6
ω_h, s^{-1}	0.36

Warburg finite–length transport layer[17]

$$\omega_{ox} \simeq \frac{2.54D_{ox}}{l_t^2}, \quad \omega_b \simeq \frac{2.54D_b}{l_b^2} \qquad [4]$$

where D_b is the effective oxygen diffusion coefficient in the GDL, and l_b is the GDL thickness. Finally, the characteristic frequency of oxygen transport in the channel is given by

$$\omega_h \simeq \frac{v}{L} \qquad [5]$$

where v is the flow velocity and L is the channel length. Typical PEMFC geometrical and operating parameters are collected in Table I; the characteristic frequencies calculated with this set of parameters are listed in the bottom part of this Table.

We see that the following relation holds: $\omega_h \ll \omega_b \simeq \omega_{ct} < \omega_{ox} \ll \omega_p$, i.e., the lowest characteristic frequency in the system is the channel–transport one, Eq. 5. This frequency is two orders of magnitude less, than the nearest frequency of oxygen transport in the GDL. Note that the charge–transfer frequency ω_{ct} is close to the channel transport frequency ω_h only if the cell current density is very low, less than 1 mA cm^{-2}. At the currents above 10 mA cm^{-2}, these processes are well separated on the frequency scale.

Model

Basic equations.—As the channel impedance is well separated on the frequency scale from the impedances due to proton and oxygen transport in the porous layers, we will ignore these processes in modeling impedance of the cell in Figure 1. Thus, the model below is based on two equations: (i) an equation for oxygen mass transport in the channel, and (ii) an equation for proton charge conservation in the CCL.

The oxygen mass balance equation in the cathode channel reads

$$\frac{\partial c}{\partial t} + v\frac{\partial c}{\partial z} = -\frac{j_0}{4Fh}, \quad c(0) = c_{ref} \qquad [6]$$

Here, $c(z)$ is the oxygen molar concentration, t is time, z is the distance along the channel, $j_0(z)$ is the local cell current density, and c_{ref} is the reference (inlet) oxygen concentration. Eq. 6 is written assuming that the oxygen transport in the GDL and CCL is fast. Due to this assumption, the right side of this equation represents the stoichiometric flow of oxygen corresponding to the local cell current density, as if the channel were directly connected to the catalyst layer. Further, we assume that the channel flow is a plug flow with the constant velocity v, which is a standard assumption in analytical modeling of PEMFCs.

The transient proton current conservation equation in the CCL is

$$C_{dl}\frac{\partial \eta}{\partial t} + \frac{\partial j}{\partial x} = -i_*\left(\frac{c}{c_{ref}}\right)\exp\left(\frac{\eta}{b}\right) \qquad [7]$$

Here, η is the ORR overpotential, positive by convention, j is the local proton current density in the CCL, x is the distance through the CCL depth, i_* is the volumetric exchange current density.

The approximation of fast proton and oxygen transport in the CCL means that η and c are nearly constant through the CCL depth, and we can integrate Eq. 7 over x from 0 to the CCL thickness l_t. This yields

$$C_{dl}l_t\frac{\partial \eta}{\partial t} - j_0 = -l_t i_*\left(\frac{c}{c_{ref}}\right)\exp\left(\frac{\eta}{b}\right) \qquad [8]$$

It is convenient to introduce dimensionless variables

$$\tilde{x} = \frac{x}{l_t}, \quad \tilde{t} = \frac{t}{t_*}, \quad \tilde{c} = \frac{c}{c_{ref}}, \quad \tilde{j} = \frac{j}{j_*}, \quad \tilde{\eta} = \frac{\eta}{b},$$
$$\tilde{z} = \frac{z}{L}, \quad \tilde{Z} = \frac{Zj_*}{b}, \quad \tilde{\omega} = \omega t_* \qquad [9]$$

where Z is the cell impedance, ω is the angular frequency of the applied signal, and

$$j_* = l_t i_*, \quad t_* = \frac{C_{dl}b}{i_*} \qquad [10]$$

are the scaling factors for current density and time, respectively. With these variables, Eqs. 6 and 8 take the form

$$\psi^2\frac{\partial \tilde{c}}{\partial \tilde{t}} + \lambda\tilde{J}\frac{\partial \tilde{c}}{\partial \tilde{z}} = -\tilde{j}_0 \qquad [11]$$

$$\frac{\partial \tilde{\eta}}{\partial \tilde{t}} - \tilde{j}_0 = -\tilde{c}\exp(\tilde{\eta}) \qquad [12]$$

where

$$\lambda = \frac{4FhvC_{ref}}{LJ} \qquad [13]$$

is the stoichiometry of the oxygen (air) flow and ψ is the constant parameter

$$\psi = \sqrt{\frac{4FhC_{ref}}{l_tC_{dl}b}} \qquad [14]$$

Impedance.—Now we can apply small–amplitude harmonic perturbations:

$$\tilde{\eta} = \tilde{\eta}^0 + \tilde{\eta}^1(\tilde{\omega})\exp(i\tilde{\omega}\tilde{t})$$
$$\tilde{c} = \tilde{c}^0(\tilde{z}) + \tilde{c}^1(\tilde{z}, \tilde{\omega})\exp(i\tilde{\omega}\tilde{t}) \qquad [15]$$
$$\tilde{j}_0 = \tilde{j}_0^0(\tilde{z}) + \tilde{j}_0^1(\tilde{z}, \tilde{\omega})\exp(i\tilde{\omega}\tilde{t})$$

where the superscripts 0 and 1 mark the steady–state solutions and the small perturbations, respectively. Note that $\tilde{\eta}^0$ and $\tilde{\eta}^1$ are independent of $\tilde{z}$, as the electric conductivity of the cell components is assumed to be large.

Substituting Eqs. 15 into 11 and 12, subtracting the respective steady–state equations, expanding the exponent on the right side of Eq. 12 and neglecting terms with the perturbation products, we get a

pair of linear equations

$$\lambda\tilde{J}\frac{\partial\tilde{c}^1}{\partial\tilde{z}} = -\left(e^{\tilde{\eta}^0} + i\tilde{\omega}\psi^2\right)\tilde{c}^1 - \left(e^{\tilde{\eta}^0}\tilde{c}^0 + i\tilde{\omega}\right)\tilde{\eta}^1, \quad \tilde{c}^1(0) = 0 \qquad [16]$$

$$\tilde{j}_0^1 = e^{\tilde{\eta}^0}\left(\tilde{c}^1 + \tilde{c}^0\tilde{\eta}^1\right) + i\tilde{\omega}\tilde{\eta}^1 \qquad [17]$$

where Eq. 16 is obtained using Eq. 17. The boundary condition to Eq. 16 means that the inlet oxygen concentration is not perturbed.

A good approximation for the static low–current shape of the oxygen concentration along the channel is[19]

$$\tilde{c}^0(\tilde{z}) = \left(1 - \frac{1}{\lambda}\right)^{\tilde{z}} \qquad [18]$$

Substituting 18 into Eq. 16 and solving Eq. 16 we get

$$\tilde{c}^1(\tilde{z},\tilde{\omega}) = -\frac{i\tilde{\omega}\tilde{\eta}^1}{p}\left(1 - \exp\left(-\frac{p\tilde{z}}{\lambda\tilde{J}}\right)\right) + \frac{\tilde{\eta}^1 e^{\tilde{\eta}^0}\left(\exp\left(-\frac{p\tilde{z}}{\lambda\tilde{J}}\right) - \left(1 - \frac{1}{\lambda}\right)^{\tilde{z}}\right)}{p + \lambda\tilde{J}\ln\left(1 - \frac{1}{\lambda}\right)} \qquad [19]$$

where

$$p \equiv e^{\tilde{\eta}^0} + i\tilde{\omega}\psi^2 \qquad [20]$$

The local impedance $\tilde{Z}_{loc}$ of the cell is

$$\tilde{Z}_{loc}(\tilde{z}) = \left.\frac{\tilde{\eta}^1}{\tilde{j}_0^1}\right|_{\tilde{x}=0} \qquad [21]$$

Substituting Eq. 19 into Eq. 17 and dividing both sides of the resulting equation by $\tilde{j}_0^1$, we find

$$\tilde{Z}_{loc} = \frac{1}{i\tilde{\omega} + Q} \qquad [22]$$

where

$$Q = \left[\left(1 - \frac{1}{\lambda}\right)^{\tilde{z}} - \frac{i\tilde{\omega}}{p}\left(1 - \exp\left(-\frac{p\tilde{z}}{\lambda\tilde{J}}\right)\right) + \frac{\left(\exp\left(-\frac{p\tilde{z}}{\lambda\tilde{J}}\right) - \left(1 - \frac{1}{\lambda}\right)^{\tilde{z}}\right)e^{\tilde{\eta}^0}}{p + \lambda\tilde{J}\ln\left(1 - \frac{1}{\lambda}\right)}\right]e^{\tilde{\eta}^0} \qquad [23]$$

It is convenient to eliminate the static overpotential $\tilde{\eta}^0$ from the equations above. At low cell currents, the local static cell current density $\tilde{j}_0^0$ depends on the coordinate $\tilde{z}$ as[19]

$$\tilde{j}_0^0 = -\lambda\tilde{J}\ln\left(1 - \frac{1}{\lambda}\right)\left(1 - \frac{1}{\lambda}\right)^{\tilde{z}} \qquad [24]$$

Further, the static local polarization curve of the cell segment is given by the Tafel law, $\tilde{j}_0^0 = \tilde{c}^0 \exp\tilde{\eta}^0$. Substituting here 24 for $\tilde{j}_0^0$ and 18 for $\tilde{c}^0$, we get the global polarization curve of the cell

$$-\lambda\ln\left(1 - \frac{1}{\lambda}\right)\tilde{J} = \exp\tilde{\eta}^0 \qquad [25]$$

which allows us to eliminate $\exp\tilde{\eta}^0$ in the equations above.

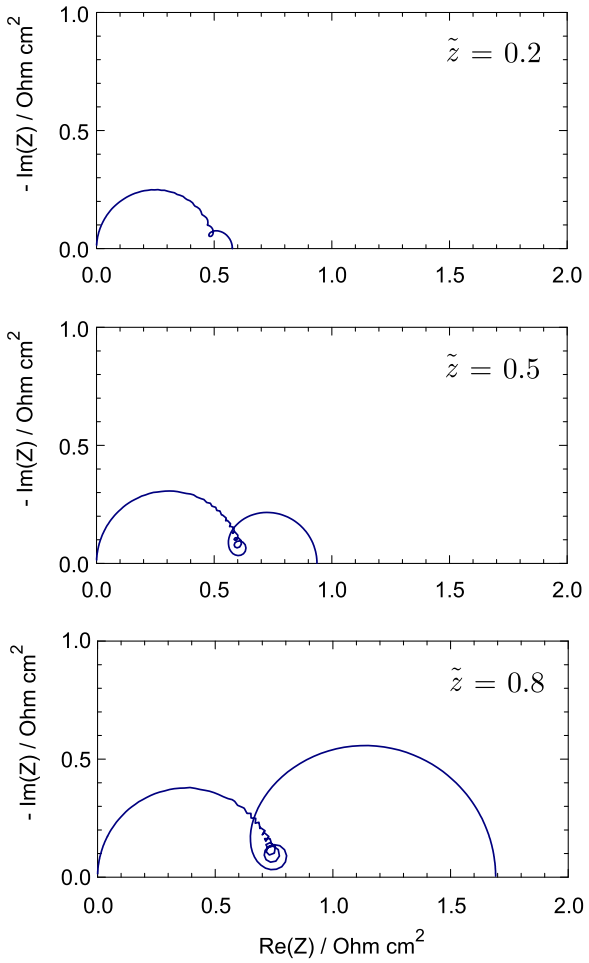

Figure 2. The spectra of Eq. 22 (local spectra) for the indicated distances from the channel inlet. Parameters for the calculations are listed in Table I.

Cell impedance.—Evidently, local impedances Eq. 22 are connected in parallel (Figure 1). Thus, the total cell impedance $\tilde{Z}_{tot}$ is given by

$$\frac{1}{\tilde{Z}_{tot}} = \int_0^1 \frac{d\tilde{z}}{\tilde{Z}_{loc}} \qquad [26]$$

Calculating integral with Eq. 22 and using Eq. 25, we come to

$$\tilde{Z}_{tot} = -\frac{i\tilde{\omega}\psi^2}{D}\left(\lambda q\tilde{J} - i\tilde{\omega}\psi^2\right)^2 \qquad [27]$$

where

$$D = \left(\lambda q\tilde{J} - i\tilde{\omega}\psi^2\right)\left(\lambda^2(\lambda-1)q^2\tilde{J}^2 - \tilde{\omega}^2\psi^4\right)\tilde{J} - \left(\tilde{\omega}^2\psi^4 + (i\tilde{\omega}\psi^2 + \lambda\tilde{J})\lambda q\tilde{J}\right)\tilde{\omega}^2\psi^2 - \left((\lambda q\tilde{J} - i\tilde{\omega}\psi^2)\lambda q\tilde{J} - \tilde{\omega}^2\psi^2\right)\lambda(\lambda-1)q\tilde{J}^2\exp\left(-\frac{i\tilde{\omega}\psi^2}{\lambda\tilde{J}}\right) \qquad [28]$$

and

$$q = \ln\left(1 - \frac{1}{\lambda}\right) \qquad [29]$$

Results and Discussion

The local spectra of Eq. 22 are shown in Figure 2 for the three distances from the channel inlet $\tilde{z} = 0.2, 0.5$ and 0.8. The low–frequency

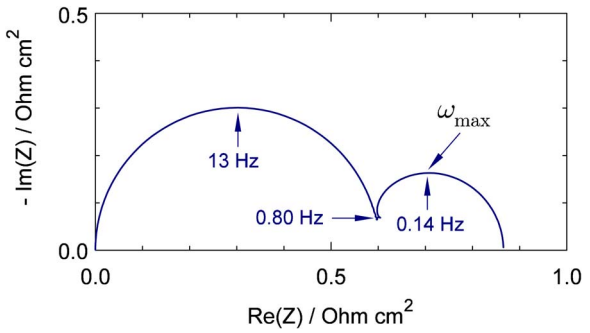

Figure 3. The spectrum of Eq. 27 (the whole cell spectrum) for the same set of parameters as in Figure 2.

arc manifests oxygen transport impedance in the air channel. The nature of impedance "loops" in Figure 2 has been discussed in Refs. 3,5. The total spectrum of the cell, Eq. 27, is depicted in Figure 3 for the same as in Figure 2 parameters.

Calculating the limit of $\lambda = \infty$ in Eq. 27, we get

$$\tilde{Z}_{ct} = \frac{1}{\tilde{J} + i\tilde{\omega}} \qquad [30]$$

Evidently, Eq. 30 is the faradaic (charge–transfer) impedance of the CCL. Subtracting $\tilde{Z}_{ct}$ from $\tilde{Z}_{tot}$, we find the pure "channel" impedance $\tilde{Z}_h$ of the cell:

$$\tilde{Z}_h = -\frac{i\tilde{\omega}\psi^2}{D}\left(\lambda q\tilde{J} - i\tilde{\omega}\psi^2\right)^2 - \frac{1}{\tilde{J} + i\tilde{\omega}} \qquad [31]$$

Numerical calculations show, that the summit frequency ω_{max} of the "channel" arc (Figure 3) is well approximated by the following relation

$$\omega_{max} \simeq -\frac{3.3J}{4Fhc_{ref}\ln\left(1 - \frac{1}{\lambda}\right)} \qquad [32]$$

Figure 4 shows the exact numerical ω_{max} calculated as a solution to equation $\partial \mathrm{Im}\,(Z_h)/\partial\omega = 0$ (open points) and the approximate analytical Eq. 32 (solid line). As can be seen, the agreement is good. For large $\lambda \gg 1$, the log–function in Eq. 32 can be expanded in Taylor series, and 32 simplifies to

$$\omega_{max} \simeq \frac{3.3\lambda J}{4Fhc_{ref}}, \quad \lambda \gg 1 \qquad [33]$$

With the definition of λ, Eq. 13, Eq. 33 reduces to

$$\omega_{max} \simeq \frac{3.3v}{L}, \quad \lambda \gg 1 \qquad [34]$$

which differs from the estimate for characteristic frequency of oxygen transport ω_h, Eq. 5, by a numeric factor 3.3.

Setting in Eq. 27 $\tilde{\omega} = 0$, we get the total static resistivity of the cell, which in the dimension form is

$$R_{tot} = -\frac{b}{(\lambda - 1)\ln\left(1 - \frac{1}{\lambda}\right)J} \qquad [35]$$

Taking into account that the faradaic resistivity is b/J, we find the static resistivity due to oxygen transport in the channel $R_h = R_{tot} - b/J$:

$$R_h = -\frac{b}{(\lambda - 1)\ln\left(1 - \frac{1}{\lambda}\right)J} - \frac{b}{J} \qquad [36]$$

This result can be obtained directly by passing to the limit $\tilde{\omega} \to 0$ in Eq. 31.

As can be seen, R_h is a function of the oxygen flow stoichiometry λ, the mean cell current density J and of the ORR Tafel slope b. Though

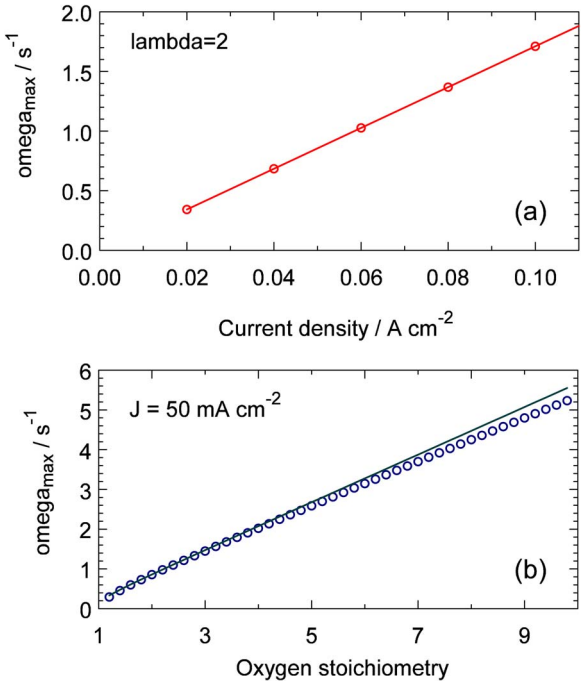

Figure 4. The exact numerical ω_{max} calculated as a solution to equation $\partial \mathrm{Im}\,(Z_h)/\partial\omega = 0$ (open points) and the approximate analytical Eq. 32 (solid line) as a function of (a) cell current density and (b) air flow stoichiometry. Parameters for the calculation are listed in Table I.

the model above ignores the oxygen and the proton transport in the porous layers, Eqs. 31 and 36 provide an accurate approximation for Z_h and R_h, respectively, provided that the characteristic frequency of oxygen transport in the channel is much less than the frequencies of the other transport processes in the cell. At small cell currents, the two orders of magnitude gap between ω_{max} and ω_b provides validity of Eq. 36 in practical applications.

It is interesting to compare R_h predicted by Eq. 36 with the experiment. Figure 5 shows the measured spectrum of a PEMFC at the cell current density of 100 mA cm^{-2} and the air flow stoichiometry $\lambda = 2$ (Ref. 6). With the Tafel slope of 31.5 mV and $\lambda = 2$, Eq. 36 gives $R_h = 0.14\ \Omega\ \mathrm{cm}^2$. This value agrees with the diameter of the LF arc in Figure 5, which is $\simeq 0.16\ \Omega\ \mathrm{cm}^2$. Note that the model[6] gives for R_h a somewhat lower value of $0.1\ \Omega\ \mathrm{cm}^2$, which can be explained by almost twice larger effective air flow stoichiometry used in Ref. 6.

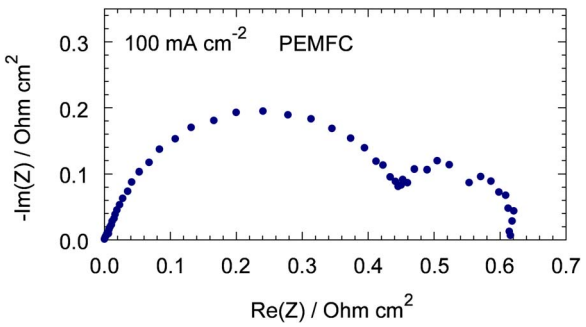

Figure 5. Measured spectrum of a PEMFC at the cell current density of 100 mA cm^{-2}. Working conditions (anode/cathode): pressure 1.5/1.5 bar, flow stoichiometry 2/2, relative humidity 100%/50%; cell temperature 80°C. Gore MEA has been used; further details are given in Ref. 18. The Tafel slope $b = 0.0315$ V has been obtained by fitting the model[6] to the spectrum.

Eqs. 31 and 36 are obtained ignoring viscous effects in the channel flow and possible formation of liquid water droplets in the channel. Thus, Eqs. 31 and 36 provide a lower, best–case estimate of the channel impedance and resistivity. In practice, if the condition $\omega_{\max} \ll \omega_b$ holds, R_h can be estimated as a diameter of LF arc in the experimental spectrum of a cell. The difference of a measured R_h and the resistivity given by Eq. 36 could give a contribution of the viscous and liquid water transport effects to the flow field resistivity. Note, however, that in some cases, the LF part of PEMFC spectra contains an inductive loop, which increases a visible diameter of the LF arc.[20] The physical nature of this loop is not quite clear; most probable explanations are slow dynamics of adsorbed ORR intermediates ,[21] or oxides[22] on a Pt surface. Thus, extraction of pure channel impedance from experimental spectra could be a non–trivial task.

Eq. 32 shows that $\omega_{\max}$ increases with J. For the cell current density on the order of 1 A cm^{-2}, $\omega_{\max}$ becomes on the order of ω_b and hence the LF arc in the cell would merge with the faradaic arc. However, large currents are out of the scope of the model above. Further, $\omega_{\max}$ increases also with the oxygen stoichiometry λ (Figure 4b. Nonetheless, in the range of typical stoichiometries ($\lambda = 1.5$ to 3) the variation of $\omega_{\max}$ with λ is small (Figure 4b).

Conclusions

A model for impedance of oxygen transport in a PEM fuel cell channel is developed. Estimates show that for low cell currents and typical PEMFC parameters and operating conditions, the characteristic frequency of oxygen transport in the channel is two orders of magnitude less than the nearest characteristic frequency of oxygen transport in the GDL. The impedance model is thus based on equations for the ion charge conservation in the cathode catalyst layer, and for the oxygen mass transport in the channel. The oxygen and proton transport in the porous layers are assumed to be fast. An analytical solution for the channel impedance Z_h is derived and a simple approximate equation for the summit frequency $\omega_{\max}$ of the transport arc in the Nyquist spectrum is obtained. In the limit of zero frequency of the AC signal, the rather cumbersome expression for Z_h leads to a simple expression for the cell resistivity due to oxygen transport in the channel.

List of Symbols

˜	Marks dimensionless variables
b	ORR Tafel slope, V
C_{dl}	Double layer volumetric capacitance, F cm^{-3}
c	Oxygen molar concentration, mol cm^{-3}
c_{ref}	Reference oxygen concentration (at the channel inlet), mol cm^{-3}
D_b	Effective oxygen diffusion coefficient in the GDL, cm^2 s^{-1}
D_{ox}	Effective oxygen diffusion coefficient in the CCL, cm^2 s^{-1}
F	Faraday constant, C mol^{-1}
f	Regular frequency, Hz
J	Mean cell current density, A cm^{-2}
j	Local proton current density in the CCL, A cm^{-2}
j_0	Local cell current density, A cm^{-2}
h	Channel depth, cm
i	Imaginary unit
i_*	Volumetric exchange current density, A cm^{-3}
L	Channel length,cm
l_b	GDL thickness, cm
l_t	Catalyst layer thickness, cm
q	Dimensionless parameter, Eq. 29
t	Time, s
v	Flow velocity in the cathode channel, cm s^{-1}
x	Coordinate through the cell, cm
Z	Impedance, Ω cm^2
z	Coordinate along the air channel, cm

Greek

λ	Air flow stoichiometry
σ_p	CCL proton conductivity, Ω^{-1} cm^{-1}
ω	Angular frequency ($\omega = 2\pi f$), s^{-1}
$\omega_{\max}$	Summit frequency of the channel impedance, s^{-1}

Subscripts

0	Membrane/CCL interface
1	CCL/GDL interface
b	GDL
h	Air channel
loc	Local impedance
ox	Oxygen
p	Proton
t	Catalyst layer
$*$	Characteristic value

Superscripts

0	Steady–state value
1	Small–amplitude perturbation

ORCID

Andrei Kulikovsky https://orcid.org/0000-0003-1319-576X

References

1. I. A. Schneider, S. A. Freunberger, D. Kramer, A. Wokaun, and G. G. Scherer, "Oscillations in gas channels. part i. the forgotten player in impedance spectroscopy in PEFCs," *J. Electrochem. Soc.*, **154**, B383 (2007).
2. I. A. Schneider, D. Kramer, A. Wokaun, and G. G. Scherer, Oscillations in gas channels. ii. unraveling the characteristics of the low–frequency loop in air–fed PEFC impedance spectra," *J. Electrochem. Soc.*, **154**, B770 (2007).
3. A. A. Kulikovsky, A model for local impedance of the cathode side of PEM fuel cell with segmented electrodes," *J. Electrochem. Soc.*, **159**, F294 (2012).
4. C. Bao and W. G. Bessler, Two–dimensional modeling of a polymer electrolyte membrane fuel cell with long flow channel. Part II. physics–based electrochemical impedance analysis," *J. Power Sources*, **278**, 675 (2015).
5. A. Kulikovsky and O. Shamardina, A model for PEM fuel cell impedance: Oxygen flow in the channel triggers spatial and frequency oscillations of the local impedance," *J. Electrochem. Soc.*, **162**, F1068 (2015).
6. A. Kulikovsky, A fast low-current model for impedance of a PEM fuel cell cathode at low air stoichiometry," *J. Electrochem. Soc.*, **164**(9), F911 (2017).
7. T. Reshetenko and A. Kulikovsky, A model for extraction of spatially resolved data from impedance spectrum of a PEM fuel cell," *J. Electrochem. Soc.*, **165**, F291 (2018).
8. S. J. C. Cleghorn, C. R. Derouin, M. S. Wilson, and S. Gottesfeld, A printed circuit board approach to measuring current distribution in a fuel cell," *J. Appl. Electrochem.*, **28**, 663 (1998).
9. D. J. L. Brett, S. Atkins, N. P. Brandon, V. Vesovic, N. Vasileadis, and A. Kucernak, Localized impedance measurements along a single channel of a solid polymer fuel cell," *Electrochem. Solid State Lett.*, **6**, A63 (2003).
10. T. V. Reshetenko, G. Bender, K. Bethune, and R. Rocheleau, A segmented cell approach for studying the effects of serpentine flow field parameters on PEMFC current distribution," *Electrochimica Acta*, **88**, 571 (2013).
11. E. Engebretsen, G. Hinds, Q. Meyer, T. Mason, E. Brightman, L. Castanheira, P. R. Shearing, and D. J. L. Brett, Localised electrochemical impedance measurements of a polymer electrolyte fuel cell using a reference electrode array to give cathode–specific measurements and examine membrane hydration dynamics," *J. Power Sources*, **382**, 38 (2018).
12. T. Holm, M. Ingdal, E. V. Fanavoll, S. Sunde, F. Seland, and D. A. Harrington, Mass–transport impedance at channel electrodes: Accurate and approximate solutions," *Electrochimica Acta*, **202**, 84 (2016).
13. S. Chevalier, C. Josset, A. Bazylak, and B. Auvity, Measurements of air velocities in polymer electrolyte membrane fuel cell channels using electrochemical impedance spectroscopy," *J. Electrochem. Soc.*, **163**, F816 (2016).
14. S. Chevalier, C. Josset, and B. Auvity, Analytical solution for the low frequency polymer electrolyte membrane fuel cell impedance," *J. Power Sources*, **407**, 123 (2018).
15. A. A. Kulikovsky, The regimes of catalyst layer operation in a fuel cell," *Electrochimica Acta*, **55**, 6391 (2010).
16. A. A. Kulikovsky and M. Eikerling, Analytical solutions for impedance of the cathode catalyst layer in PEM fuel cell: Layer parameters from impedance spectrum without fitting," *J. Electroanal. Chem.*, **691**, 13 (2013).
17. J. R. Macdonald, *Impedance Spectroscopy*. Wiley, New York, 1987.
18. T. Reshetenko and A. Kulikovsky, Comparison of two physical models for fitting PEM fuel cell impedance spectra measured at a low air flow stoichiometry," *J. Electrochem. Soc.*, **163**, F238 (2016).

19. A. A. Kulikovsky, The effect of stoichiometric ratio λ on the performance of a polymer electrolyte fuel cell," *Electrochimica Acta*, **49**(4), 617 (2004).
20. I. Pivac, B. Simic, and F. Barbir, Experimental diagnostics and modeling of inductive phenomena at low frequencies in impedance spectra of proton exchange membrane fuel cells," *J. Power Sources*, **365**, 240 (2017).
21. S. K. Roy, M. E. Orazem, and B. Tribollet, Interpretation of low-frequency inductive loops in pem fuel cells," *J. Electrochem. Soc.*, **154**, B1378 (2007).
22. B. P. Setzler and Th. F. Fuller, A physics–based impedance model of proton exchange membrane fuel cells exhibiting low–frequency inductive loops," *J. Electrochem. Soc.*, **162**, F519 (2015).